Philosophical Magazine Letters in press (2010)

Role of Surface Roughness in Hysteresis during Adhesive Elastic Contact

Haneesh Kesari[a], Joseph C. Doll[a], Beth L. Pruitt[a], Wei Cai[a], and Adrian J. Lew[a] *

[a]*Department of Mechanical Engineering, Stanford University, Stanford, CA, 94305-4040*

(*April 2010*)

In experiments that involve contact with adhesion between two surfaces, as found in atomic force microscopy or nanoindentation, two distinct contact force (P) vs. indentation-depth (h) curves are often measured depending on whether the indenter moves towards or away from the sample. The origin of this hysteresis is not well understood and is often attributed to moisture, plasticity or viscoelasticity. Here we report experiments that show that hysteresis can exist in the absence of these effects, and that its magnitude depends on surface roughness. We develop a theoretical model in which the hysteresis appears as the result of a series of surface instabilities, in which the contact area grows or recedes by a finite amount. The model can be used to estimate material properties from contact experiments even when the measured P-h curves are not unique.

Keywords: atomic force microscopy, nanoindentation, surface roughness, adhesion, contact mechanics.

1. Introduction

Adhesive contacts play a central role in many biological phenomena and engineered systems, such as in cell adhesion [1] and microdevices [2]. In particular, characterization of materials using contact experiments, such as Atomic Force Microscopy (AFM), requires an understanding of adhesive contacts [3–5]. During adhesive contact the measured contact force vs. indentation-depth (P-h) curves often display a clear and repeatable hysteresis loop [4, 6–9] (Fig. 1(a)). These curves have two branches, one measured as the indenter moves towards the sample, and another one as it moves away. The area inside the hysteresis loop ($\mathcal{H}$) measures the energy loss during a cycle. In some adhesive contact experiments [such as, 4, 6–9, and this study], $\mathcal{H}$ depends on the maximum indentation-depth, $|h_{\min}|$. We refer to this behavior as depth-dependent hysteresis (DDH).

DDH cannot be explained by classical contact theories [10–13], which predict a P-h curve with a single branch in the regime of $h < 0$. Fitting experimental data displaying DDH to these theories leads to different estimates for material properties depending on which branch of the curve is used [8, 9, 14, 15]. The mechanism of DDH is not well understood, but it has been attributed to several factors, such as material damage (plasticity) [16], ambient moisture [6, 17], viscoelasticity [18], and chemistry related mechanisms [7–9, 19]. Here, we report experiments in which the observed DDH cannot be explained by these factors alone. Furthermore, the observed DDH is found to depend on surface roughness. Thus, we hypothesize that

*Corresponding author. Email: lewa@stanford.edu, Ph: +1 (650) 725-3585, Fax: +1 (650) 723-1778

ISSN: 0950-0839 print/ISSN 1362-3036 online

DOI: 10.1080/0950083YYxxxxxxxx
http://www.informaworld.com

surface roughness coupled with adhesion can give rise to DDH. We also present a model for adhesive elastic contact between rough surfaces whose predictions are consistent with our experiments. Most notably, it predicts different P-h branches during loading and unloading. Therefore, our model enables the estimation of material properties by simultaneously fitting both branches of the experimental P-h curves, instead of having to choose among the two. The fitting also provides certain information about surface roughness of the contacting surfaces.

2. Materials and Methods

2.1. *Hysteresis measurements*

To investigate the mechanism of DDH we measured P-h curves on four Polydimethylsiloxane (PDMS) samples having varying roughness using both AFM and nanoindentation apparatus. The AFM tip was a spherical glass bead and the nanoindentation tip was a flat face of a truncated diamond cube. Details of PDMS sample preparation, AFM, and nanoindentation experiments are given in the following sections.

On each sample we measured P-h curves at five different sample spots that were separated from one another by at least $200\,\mu$m. We brought the tip into contact with each sample spot several times (≈ 20); each time starting from a tip-sample separation where $P = 0$. The tip base was moved towards the samples until the tip was pushed into the sample by a predetermined amount—the maximum indentation-depth ($|h_{min}|$)—and then moved away until $P = 0$ again. We counted each time the tip is brought into contact with the sample as a contact cycle. The speed of the tip's base ($\dot{d}$) was kept constant during the measurements. As stated, at each sample location we performed several contact cycles with $|h_{\min}|$ ranging from 0 to 1500 nm. For each $|h_{\min}|$, we calculated the energy loss $\mathcal{H}$ by computing the area enclosed within the corresponding contact cycle's P-h loop.

For a given $|h_{\min}|$, the $\mathcal{H}$ for a sample is the average of the data taken at the five locations. The error bars for $\mathcal{H}$ are the standard deviation of the data taken over the five locations.

2.2. *Polydimethysiloxane (PDMS) sample preparation*

We fabricated PDMS samples having varying roughness but identical mechanical properties and surface chemistry using a soft-lithography technique [20], where the same PDMS solution (base:crosslinker= 10:1, Sylgard 184, Dow Corning, Midland, MI) was cast onto different silicon (Si) molds (University Wafer, South Boston, MA). The Si molds were roughened to varying extents by exposing them to reactive ions in a parallel plate plasma etcher (RIE-100, Drytek) for durations ranging from 30 seconds to 6 minutes. The gas flow rates (SF_6/O_2 = 90/25 sccm), RF power (200 W), and pressure (70 mTorr) were held constant for all etches. The PDMS solution was well mixed and deaerated in a centrifugal mixer (AR-100, Thinky, Tokyo, Japan) to obtain a uniformly mixed prepolymer solution. The Si molds were vapor coated with a releasing agent (Chlorotrimethylsilane, Sigma-Aldrich, St. Louis, MO) before casting a 5-10 mm thick prepolymer solution onto them. Vacuum was applied to the casts for 15 minutes before curing them at room temperature ($\approx 20^\circ$ C) for 48 hours.

We measured the Si molds topography by scanning their surfaces using a sharp Si tipped AFM operated in tapping mode. We performed these measurements over $4\,\mu m^2$ scan areas at three different locations on each sample. From these

measurements, we observed that the Si molds RMS (root mean square) roughness varied from 0.65 to 1.52 nm. The number of asperities, which we determined by counting the points where the topography had a local maxima, were 213 ± 10, 99 ± 8, 98 ± 8, and 75 ± 4 per square micron on the Si wafers exposed to 0 sec, 30 sec, 3 min, and 6 min of reactive ion etching respectively.

Because of the large compliance of PDMS (Young's modulus ~ 1 MPa), we could not measure the PDMS sample roughness directly using an AFM. However, the soft-lithography technique we used [20] is known to replicate features down to 2 nm [21]. Thus, in this work we assume that the RMS roughness of our PDMS samples is proportional to that of their respective Si molds on which they were cast. Furthermore, since the different PDMS samples were cast from the same prepolymer solution we expect that all samples have the same bulk mechanical properties and surface chemistry.

2.3. *Atomic Force Microscope (AFM) Contact Experiments*

Indentation with soda lime glass beads (Duke Scientific, Palo Alto, USA) was performed in air at room temperature using an AFM (alpha300A, Witec Instruments, Ulm, Germany) operated in the contact mode. The beads had a diameter of 50 μm, and a RMS roughness of 6 nm. They were attached onto an AFM cantilever (Arrow NCR, Nanoworld, Neuchâtel, Switzerland) using epoxy resin. The spring constant of the cantilever was estimated to be 30 ± 6 N/m by measuring the resonant frequency, for details see [22].

Underwater measurements were performed by placing the samples in a container filled with deionized water. At the beginning of the experiment the AFM tip was lowered into the container such that it was completely under water .

2.4. *Nanoindentation experiments*

To estimate the viscoelasticity of our PDMS samples we also measured P-h curves on all our PDMS samples using a flat faced diamond tip. These measurements were performed using a nanoindentation apparatus (Hysitron, Minneapolis, USA). The tip is a corner of a diamond cube whose apex has been flattened. The RMS roughness of the diamond tip measured through imprints on a gold surfaces was < 1 nm. The flat contacting face is an equilateral triangle with sides 10.5 μm long and an area of 47 μm^2. The machine was operated in displacement control mode.

3. Results & Discussion

3.1. *AFM Experiments*

Fig. 1 (a) shows the P-h curves using an AFM during glass-PDMS contact at the loading rate $\dot{d} = 10\,\mathrm{nm \cdot s^{-1}}$. Two distinct P-h branches are found for the loading and unloading stages. Fig. 1(b) shows that the energy loss $\mathcal{H}$ of a contact cycle increases with $|h_{\min}|$, which is a signature of depth-dependent hysteresis (DDH). Fig. 1 (c) and (d) show that similar behavior is also observed at a faster loading rate of $\dot{d} = 1000\,\mathrm{nm \cdot s^{-1}}$. For a given maximum indentation depth $|h_{\min}|$, the energy loss is larger at the higher loading rate. This rate dependence will be discussed further in Sec. 3.2.

At the higher loading rate of $\dot{d} = 1000\,\mathrm{nm \cdot s^{-1}}$, we measured the energy loss as a function of $|h_{\min}|$ on PDMS samples with different surface roughness but similar bulk properties and surface chemistry (see Sec 2.2). We chose to use the higher

loading rate in order to expedite the experiments and reduce any instrumentation drift errors in our measurements. Fig. 1 (d) shows that for a given maximum indentation depth, $\mathcal{H}$ increases as the sample RMS roughness grows from 0.65 nm to 1.31 nm, but then decreases as RMS roughness increases further to 1.52 nm. These data are also plotted in Fig. 2 (a) with RMS roughness as the x-axis. This behavior of initial increase and then decrease of $\mathcal{H}$ with RMS roughness was observed using two different sets of PDMS samples, AFM cantilevers, and glass beads on two different days. The two sets of PDMS samples were prepared using the same set of Si molds.

Ambient moisture can cause DDH because condensation of a liquid meniscus at the contact periphery is known to change the contact forces [23, pp. 880]. To test this possibility, we performed glass bead-PDMS contact experiments under water, where no meniscus can form. Fig. 1(e) and (f) show that DDH still appears in this experiment. We estimated the contributions to DDH from water's viscosity to be negligible ($\sim$ attojoules) for the loading rates used in our experiments. This is confirmed by the flat region of the P-h curve in Fig. 1(e) at $h > 0$, which indicates that no appreciable force was measured while the cantilever moves in water before touching the sample. Hence, we expect the same mechanisms causing DDH in the in-air experiments are responsible for DDH in the under water experiments as well. In addition, moisture contribution in our in-air AFM experiments, shown in Fig. 1(a-d), should be negligible since PDMS is known to be hydrophobic [24], and these experiments were performed at conditions (relative humidity 34% , temperature 23° C) at which moisture condensation is estimated to be negligible. Hence, we can rule out the possibility of moisture as the main cause of DDH in the experiments shown in Fig. 1.

To test the possibility that the observed DDH may be instrumentation artifacts, we performed glass-on-glass indentation experiments both before and after the in-air and under water glass-PDMS experiments. No sign of DDH was observed in the glass-on-glass experiments, which rules out instrumentation artifacts as a cause of the observed DDH. Furthermore, successive P-h loops measured while indenting the same sample spot to the same $|h_{\min}|$ always overlapped. We therefore exclude material damage as a plausible cause of DDH in our experiments.

3.2. *Nanoindentation Experiments*

Viscoelasticity of the sample can cause DDH [25]. To test this possibility, we indented our PDMS samples with a flat tip so that the contact area remained constant during the experiment. Flat faced tips are not standard for an AFM apparatus. However, a nanoindentation (NI) apparatus (see Sec. 2.4) with flat faced diamond tips was readily available. Although the glass-PDMS adhesion energy is different from that of diamond-PDMS [1], when the contact area remains constant the adhesion energy should not affect the contact forces.

The maximum-indentation depth, indentation rates and size of contact region in the NI experiments were chosen such that bulk deformation and deformation rates in the NI and AFM experiments were comparable. The $|h_{\min}|$ in both the AFM and the NI experiments lay in the range of $\sim$ 250-1500 nm. The contact area in the NI experiments remained constant at 47 μm^2, while that in the AFM experiments varied from 10 to 230 μm^2 as h went from 0 to 1000 nm. The loading rates,

[1] In this work we estimate glass-PDMS adhesion energy to be 26 mJ/m^2 (sec. 3.4). Cao et. al. report the diamond-PDMS adhesion energy to be 227 mJ/m^2. However, from other sources the glass-PDMS adhesion energy is seen to lie in the range 12–150 mJ/m^2 [6, 26], and the diamond-PDMS adhesion energy is seen to lie in the range 20–500 mJ/m^2 [27–29].

$\dot{d}$, in both AFM and NI experiments were varied in the range 10-1000 $\mathrm{nm \cdot s^{-1}}$. Note however that the base-tip stiffness in the NI experiments is effectively infinite compared to the stiffness of the AFM cantilever. Thus, the deformation rates in the NI experiments are expected to be somewhat larger than those in the AFM experiments for the same $\dot{d}$.

At the loading rate $\dot{d} = 10\,\mathrm{nm \cdot s^{-1}}$, the *P-h* measurements from our nanoindentation experiments did not display any appreciable hysteresis, with $\mathcal{H} < 0.03\,\mathrm{pJ}$. At the higher loading rate of $\dot{d} = 1000\,\mathrm{nm \cdot s^{-1}}$, hysteresis was observed and was found to increase with the maximum indentation depth $|h_{\min}|$. However, this depth-dependent hysteresis (DDH) was insensitive to the sample roughness, as shown in Fig. 2 (b). The NI *P-h* measurements were quite repeatable, i.e., repeatedly indenting a sample spot to the same $|h_{\min}|$ gave indistinguishable *P-h* curves. Thus, material damage can be ruled out as playing any role in these experiments. In addition, before indenting PDMS, indenting polycarbonate samples using the same NI apparatus showed no hysteresis at all. This shows that the NI apparatus did not have any intrinsic hysteresis associated with it. Thus, the DDH seen in the NI experiments is likely due to the viscoelasticity of the PDMS samples.

Since the NI experiments at $\dot{d} = 10\,\mathrm{nm \cdot s^{-1}}$ showed negligible viscoelasticity effect, the DDH seen in the AFM experiments at the same low loading rate cannot be explained by viscoelasticity. The NI experiments at $\dot{d} = 1000\,\mathrm{nm \cdot s^{-1}}$ imply that some fraction of the DDH seen in the AFM experiments at this rate is due to PDMS' viscoelasticity. However, since DDH in the NI experiments did not depend on the sample's roughness, a fraction of the DDH seen in the AFM experiments at $\dot{d} = 1000\,\mathrm{nm \cdot s^{-1}}$, specifically, the amount that varies with roughness, cannot be explained solely by PDMS' viscoelasticity.

Therefore, our study shows that there is an additional, yet unaccounted, source of DDH in our AFM experiments. Because the primary difference between the AFM and NI experiments is whether the contact area changes or remains fixed, this unaccounted source of DDH suggests a surface-related mechanism that operates when the contact area changes. This hypothesis is reinforced from the observation that $\mathcal{H}$ in the AFM experiments initially increases and then decreases with the sample's roughness. In the next section, we explore this hypothesis in depth by developing an analytic model of adhesive contact that accounts for surface roughness.

3.3. *Theory: A Model for Adhesive Elastic Contact between Rough Surfaces*

The correlation between DDH and surface roughness suggests that DDH may be *explained in terms of surface roughness*, in the absence of all the other aforementioned factors such as moisture, plasticity, viscoelasticity, etc. In the following we develop such a theory, and answer the following two questions. First, how can roughness cause DDH? Second, why does the energy loss first increase and then decrease with increasing RMS roughness?

To some extent, the effect of roughness on DDH is surprising, since the RMS roughness of the surfaces of the samples and the indenter (a few nm) is significantly smaller than the radius of the contact region in our experiments (2 to 8.5 μm). In many situations the effect of such small surface perturbations on $\mathcal{H}$ are negligible, such as in the NI experiments in Fig. 2(b) (see also [30]). As we discuss next, however, surface roughness can change how the contact area *evolves* with h, and hence exert a dramatic influence on $\mathcal{H}$ as shown in Fig. 2(a).

During a slow loading (unloading) process, the contact area grows (decreases) in a way that is always in equilibrium: changes in elastic and interfacial energies induced by small variations of the contact area exactly balance. When the surfaces

are perfectly smooth, only one equilibrium contact area exists for each h. However, multiple equilibria can exist if the surfaces are rough. Among these equilibria, those with smaller contact areas are probed while loading, while equilibria with larger contact areas are explored during unloading. This leads to two different P-h curves for the loading and unloading phases, and is sufficient to cause DDH.

To quantify the magnitude of the energy loss due to roughness, we consider the contact between a rigid spherical indenter with radius R and a wavy sample surface with wave length λ and amplitude $2A$ (Fig. 3(c)). The RMS roughness of this model surface is proportional to A. In the following we find that, as A grows, $\mathcal{H}$ increases when A is small, and decreases when A is large, in agreement with our experimental observations.

We first assume that A is small enough such that the contact area between the two bodies is simply connected, i.e, within the contact area the surfaces adhere uniformly leaving no gaps (*small roughness* in Fig. 2 (a)). When the surface shape of the sample is an axi-symmetric sinusoid, the equilibrium P–h curve has been analytically derived in [31], Eqs. (2), (3), in [14].

Examples of this equilibrium P–h curve are shown in Fig. 3 (a), (b), as solid gray curves. The equilibrium P–h curve has oscillations, or folds, owing to the sinusoidal topography of the surfaces. In some cases (such as those shown in Fig. 3) the oscillations can be so pronounced that multiple values of P appear for each h, each one the consequence of a different equilibrium contact area. This phenoemenon has been discussed in [31], and explored experimentally at the macroscale ($\sim 10^{-2}$ m) in [14].

We construct a model for roughness by first deriving asymptotic forms for Eqs. (2), (3), of [14] and then using them to derive the equations for the *measured* P–h curve. Specifically, as we will show elsewhere, when $\lambda/R \ll 1$ and $A/\lambda \sim O(1)$, the $P(h)$ curve is multiply valued. Consequently, the P–h curve measured in an experiment does not follow the folds of the equilibrium P–h curve, but depends on the loading history (e.g., the thin solid red curve in Fig .3 (a)). As λ/R decreases, the folds in Fig. 3 (a) get tighter, see Fig. 3 (b). Under these conditions, an experimentally measured P–h loop will essentially follow the envelope of the folded analytic curve, given by [1],

$$P(a) = \frac{4E^*}{3R}a^3 - \sqrt{8\pi\gamma E^*}a^{\frac{3}{2}} \pm 2\pi E^* \frac{A}{\lambda^{1/2}}a^{\frac{3}{2}}, \tag{1a}$$

$$h(a) = \frac{1}{R}a^2 - \sqrt{\frac{2\pi\gamma}{E^*}}a^{\frac{1}{2}} \pm \pi\frac{A}{\lambda^{1/2}}a^{\frac{1}{2}}. \tag{1b}$$

This envelope is parameterized by the radius a of the contact area. The shape of the envelope depends on the adhesion energy between the bodies γ and the plain-strain Young's modulus E^*. The $+$ and $-$ signs corresponds to the loading and unloading phases of the experiment, respectively. When unloading begins, the experiment will initially sample a leg of the very last fold, which for $\lambda \ll R$ becomes a straight line. An example of the envelope curve is shown in Fig. 3(b) (solid blue curve).

Notice that when $A = 0$, the loading and unloading branches in (1a) and (1b) collapse to a single curve, the equilibrium P–h curve given by the JKR contact

[1]The derivation of eqs. (1a) and (1b) requires considerable space to be properly explained, so it will be published separately. Briefly, however, when $\lambda/R \ll 1$ and $A/\lambda \sim O(1)$, the equilibrium P–h curve given by Eqs. (2), (3) in [14], which are parametric equations of the form $P(a)$, $h(a)$, reduces to a form which contains terms given by the JKR contact theory and additional oscillatory terms arising due to the sinusoidal topography. We derive the equation for the envelope by replacing the oscillatory terms with their respective maximum and minimum values.

theory [10]. The JKR theory also considers adhesive contact between a paraboloid and a half-space, but ignores the roughness of the surfaces. Similarly, when both A and γ are set to 0, Eqs. (1a) and (1b) reduce to the equilibrium P–h curve given by Hertz contact theory [11], which ignores both adhesion and roughness.

3.4. *Comparing Theory with AFM experiments*

A comparison of the experimental results with a fitting to Eqs. (1a) and (1b) is shown as dashed lines in Fig. 1(a). For the fitting we used E^* for PDMS as 0.75 MPa, γ for glass-PDMS contact as 2.6×10^{-2} J and $A/\sqrt{\lambda} = 9 \times 10^{-6}\,\sqrt{\mathrm{m}}$. These values for E^* and γ are very close to the reported values [5, 6, 32, 33] for the same composition of PDMS and glass used in this work (Sec. 2.2). Additionally, the value of $A/\sqrt{\lambda}$ is commensurate with AFM scans of the glass bead, and the Si mold surfaces, which revealed a combined RMS-roughness of the bead and the samples of ~ 10 nm (A) and feature sizes smaller than 1000 nm (λ).

It follows from Eqs. (1a) and (1b) that $\mathcal{H}$ scales as $(\gamma E^*/\lambda)^{1/2}\, R\, A\, |h_{\min}|$. This means that in the small roughness limit $\mathcal{H}$ increases with the roughness A, maximum indentation depth $|h_{\min}|$, and adhesion energy γ, all consistent with our experiments. First, Fig. 2(a) shows that $\mathcal{H}$ initially increases with RMS roughness. This finding contrasts the traditional viewpoint in which the pull-off adhesion force decreases with roughness [15]. It may also explain why rolling friction initially increases with roughness, as found by Briggs and Briscoe [34], and first noted in [31]. Second, Fig. 1(b), (d), and (f) show that $\mathcal{H}$ increases linearly with $|h_{\min}|$ as predicted by our model. Finally, Fig. 1(c) and (e) show that contact forces under water are larger compared to in air, indicating that the glass-PDMS adhesion energy γ is lower under water[1]. Based on this, our model would predict that the energy loss $\mathcal{H}$ is also lower under water than in air, which is consistent with Fig. 1(d) and (f).

We should not expect $\mathcal{H}$ to always increase with A, since for A large enough the contact region ceases to be simply connected. The transition from a simply to a multiply connected contact region for a simpler geometry is known to depend on the parameter $\alpha = \sqrt{\pi^2 A^2 E^*/2\lambda\gamma}$ [30], with the contact region being simply connected for $\alpha < 1$ and multiply connected otherwise. Based on our fitted parameters, we find $\alpha \approx 0.1$. Therefore, it is reasonable to speculate that the change in trend in DDH at the largest roughness shown in Fig. 2(a) is due to a transition from only a few to many patches out of contact within the apparent contact region.

For A large enough, the two bodies are actually in contact only in small patches within the contact region (*large roughness* in Fig. 2(a)), and the elastic interactions among them are negligible. Each patch then attaches/detaches through pull-in/pull-out instabilities, as predicted by classical contact mechanics theories [10]. The value of $\mathcal{H}$ in this case is determined by the amount of energy lost at each contact patch, times the number of patches. For a sample surface shaped as a sinusoidal egg box, $\mathcal{H}$ scales as[2] $(\lambda/E^*)^{2/3}\, \gamma^{5/3}\, R\, A^{-4/3}\, |h_{\min}|$. This predicts that $\mathcal{H}$ is of the order of pJ, that it should decrease with A, and that it scales linearly with $|h_{\min}|$, all consistent with our experiments.

[1] Reduced adhesion under water has also been observed between mica surfaces [35].
[2] The derivation of this expression will be published elsewhere.

4. Conclusions

Our experiments and theoretical model suggest that in some experiments surface roughness alone coupled with adhesion can give rise to depth dependent hysteresis. A limitation of our work is that we did not have precise control of surface roughness which we could vary only in an average way. For this reason we could not directly measure an effective A or λ for our surfaces. This is important, since it seems unlikely that a single parameter, in this case the RMS roughness, would suffice to completely capture surface topography's effect on the mechanics of contact. Thus, a useful direction to pursue would be to make samples with tailored topographies and then study the effect of surface topography on contact phenomenon in more detail. Nonetheless, the current study clearly demonstrates that surface topography can give rise to depth dependent hysteresis during contact. Our study demonstrates that when there is evidence to suggest that surface roughness is responsible for the observed DDH, then materials properties, such as E^* and γ, can be estimated by simultaneously using both branches of the P-h curve. It is somewhat surprising that while the sample surfaces likely have complicated surface topographies, the fit to Eqs. (1a) and (1b), which are derived by assuming a sinusoidal surface shape, produces values for the mechanical properties that are in the range of expected values. These results are encouraging, but further exploration and validation are needed to test the robustness of this procedure to extract mechanical properties from AFM experiments. Our findings also demonstrate the possibility of extracting information about surface roughness at the nanoscale (the value of $A/\sqrt{\lambda}$) even from experiments employing micrometer-sized AFM probes.

Acknowledgements

This work is partly supported by the Center for Probing the Nanoscale (CPN), an NSF NSEC, NSF Grant No. PHY-0425897, by the NSF Career programs CMS-0547681, ECS-0449400 and CMMI-0747089, NIH R01-EB006745, and by the NSF award CNS-0619926 for computer resources. J.C.D. is supported in part by NSF and NDSEG Graduate Research Fellowships. H. K. is supported by the Herbert Kunzel Stanford Graduate Fellowship and he thanks Dr. Björn Backes for helping perform the nanoindentation experiments.

References

[1] Y. Chu et al., *Johnson-Kendall-Roberts theory applied to living cells*, Physical review letters 94(2) (2005), p. 28102. 1

[2] F. DelRio et al., *The role of van der Waals forces in adhesion of micromachined surfaces*, Nature Materials 4 (2005), pp. 629–634. 1

[3] E. Dimitriadis et al., *Determination of elastic moduli of thin layers of soft material using the atomic force microscope*, Biophysical Journal 82(5) (2002), pp. 2798–2810. 1

[4] O. Sahin et al., *An atomic force microscope tip designed to measure time-varying nanomechanical forces*, Nature 2 (2007), pp. 507–514. 1

[5] S. Park, M. Goodman, and B. Pruitt, *Analysis of nematode mechanics by piezoresistive displacement clamp*, Proceedings of the National Academy of Sciences 104(44) (2007), pp. 17376–17381. 1, 3.4

[6] J. Pickering, D. Van Der Meer, and G. Vancso, *Effects of contact time, humidity, and surface roughness on the adhesion hysteresis of polydimethylsiloxane*, Journal of Adhesion Science and Technology 15(12) (2001), pp. 1429–1441. 1, 1, 3.4

[7] N. Maeda et al., *Adhesion and Friction Mechanisms of Polymer-on-Polymer Surfaces*, Science 297(5580) (2002), pp. 379–382. 1

[8] Y. Chen, C. Helm, and J. Israelachvili, *Molecular Mechanisms Associated with Adhesion and Contact Angle Hysteresis of Monolayer Surfaces*, Journal of Physical Chemistry 95 (1991), pp. 10736–10746. 1

[9] G. Choi, S. Kim, and A. Ulman, *Adhesion Hysteresis Studies of Extracted Poly(dimethylsiloxane) Using Contact Mechanics*, Languir 13 (1997), pp. 6333–6338. 1

[10] K.L. Johnson, K. Kendall, and A.D. Roberts, *Surface Energy and the Contact of Elastic Solids*, Proceedings of the Royal Society of London. Series A, Mathematical and Physical Sciences 324(1558) (1971), pp. 301–313. 1, 3.3, 3.4, 3

[11] H. Hertz, *On the Contact of Elastic Solids*, J. Reine Angew. Math. 92 (1881), pp. 156–171. 3.3

[12] B.V. Derjaguin, V.M. Muller, and Y.P. Toporov, *Effect of Contact Deformations on the Adhesion of Particles*, Journal of Colloid and Interface Science 53(2) (1975), pp. 314–326.

[13] D. Maugis *Contact Adhesion and Rupture of Elastic Solids*, Solid State Sciences Springer, 2000. 1

[14] P. Guduru and C. Bull, *Detachment of a rigid solid from an elastic wavy surface: Experiments*, Journal of the Mechanics and Physics of Solids 55(3) (2007), pp. 473–488. 1, 3.3, 1

[15] B. Zappone, K. Rosenberg, and J. Israelachvili, *Role of nanometer roughness on the adhesion and friction of a rough polymer surface and a molecularly smooth mica surface*, Tribology Letters 26(3) (2007), pp. 191–201. 1, 3.4

[16] W. Oliver and G. Pharr, *Improved technique for determining hardness and elastic modulus using load and displacement sensing indentation experiments*, Journal of Materials Research 7(6) (1992), pp. 1564–1583. 1

[17] J. Grobelny et al., *Quantification of the meniscus effect in adhesion force measurements*, Applied Physics Letters 88 (2006), p. 091906. 1

[18] M. Giri, D. Bousfield, and W. Unertl, *Dynamic contacts on viscoelastic films: work of adhesion*, Langmuir 17(10) (2001), pp. 2973–2981. 1

[19] H. She, D. Malotky, and M. Chaudhury, *Estimation of Adhesion Hysteresis at Polymer/Oxide Interfaces Using Rolling Contact Mechanics*, Langmuir 14(11) (1998), pp. 3090–3100. 1

[20] Y. Xia and G. Whitesides, *Soft lithography*, Annual Review of Materials Science 28(1) (1998), pp. 153–184. 2.2

[21] F. Hua et al., *Polymer imprint lithography with molecular-scale resolution*, Nano Lett 4(12) (2004), pp. 2467–2471. 2.2

[22] N. Burnham et al., *Comparison of calibration methods for atomic-force microscopy cantilevers*, Nanotechnology 14(1) (2003), pp. 1–6. 2.3

[23] B. Bhushan *Springer handbook of nanotechnology*, Springer, 2006. 3.1

[24] J. McDonald et al., *Fabrication of microfluidic systems in poly (dimethylsiloxane)*, Electrophoresis 21(1) (1999), pp. 27–40. 3.1

[25] Y.Y. Lin and C.Y. Hui, *Mechanics of Contact and Adhesion between Viscoelastic Spheres: An Analysis of Hysteresis during Loading and Unloading*, Journal of Polymer Science: Part B: Polymer Physics 40 (2002), pp. 772–793. 3.2

[26] A. Sofla et al., *PDMS-Glass Interface Adhesion Energy Determined Via Comprehensive Solutions for Thin Film Bulge/Blister Tests*, Journal of Applied Mechanics 77 (2010), p. 031007. 1

[27] C. Buchko et al., *Mechanical properties of biocompatible protein polymer thin films*, J. Mater. Res 15(1) (2000), p. 231. 1

[28] L. Bes et al., *Poly (methylmethacrylate-dimethylsiloxane) triblock copolymers synthesized by transition metal mediated living radical polymerization: bulk and surface characterization*, European Polymer Journal 39(1) (2003), pp. 5–13.

[29] A. Bietsch and B. Michel, *Conformal contact and pattern stability of stamps used for soft lithography*, Journal of Applied Physics 88 (2000), p. 4310. 1

[30] K. Johnson, *The adhesion of two elastic bodies with slightly wavy surfaces*, International Journal of Solids and Structures 32(3) (1995), pp. 423–430. 3.3, 3.4

[31] P. Guduru, *Detachment of a rigid solid from an elastic wavy surface: Theory*, Journal of the Mechanics and Physics of Solids 55(3) (2007), pp. 445–472. 3.3, 3.4

[32] F. Schneider et al., *Mechanical properties of silicones for MEMS*, Journal of Micromechanics and Microengineering 18(6) (2008), p. 065008. 3.4

[33] X. Brown, K. Ookawa, and J. Wong, *Evaluation of polydimethylsiloxane scaffolds with physiologically-relevant elastic moduli: interplay of substrate mechanics and surface chemistry effects on vascular smooth muscle cell response*, Biomaterials 26(16) (2005), pp. 3123–3129. 3.4

[34] G. Briggs and B. Briscoe, *Effect of surface roughness on rolling friction and adhesion between elastic solids*, Nature 260(5549) (1976), pp. 313–315. 3.4

[35] H. Christenson, *Adhesion and surface energy of mica in air and water*, The Journal of Physical Chemistry 97(46) (1993), pp. 12034–12041. 1

Figure captions

Figure 1. caption

(a) AFM contact force (P) as a function of indentation-depth (h) during glass-PDMS contact in air at an indenting rate of $\dot{d} = 10\,\mathrm{nm}\cdot\mathrm{s}^{-1}$. The PDMS sample was cast on a Si wafer with an RMS roughness of 1.31 nm. The dashed lines in (a) are the P-h curves predicted by Eqs. (1a) and (1b). (b) The energy loss $\mathcal{H}$ as a function of the maximum indentation-depth $|h_{\min}|$ obtained from the P-h curves shown in (a). (c) AFM P-h curve during glass-PDMS contact in air at $\dot{d} = 1000\,\mathrm{nm}\cdot\mathrm{s}^{-1}$. The PDMS sample was cast on a Si wafer with an RMS roughness of 0.65 nm. (d) The energy loss $\mathcal{H}$ as a function of $|h_{\min}|$ for indentation conditions similar to (c) on several PDMS samples cast on Si wafers with different RMS roughness (indicated next to each curve). Each curve corresponds to a different PDMS sample and was computed from measurements at five different locations on the sample. The shaded region around each curve indicates the standard deviation of the measurements taken at five locations on the PDMS samples. At each location $\mathcal{H}$ was measured for ≈ 20 different $|h_{\min}|$, for additional details see 2.1. (e) AFM P-h curve during glass-PDMS contact under water at $\dot{d} = 1000\,\mathrm{nm}\cdot\mathrm{s}^{-1}$. The PDMS sample was cast on a Si wafer with an RMS roughness of 0.65 nm. (f) The energy loss $\mathcal{H}$ as a function of $|h_{\min}|$ obtained from (e).

Figure 2. caption

Energy loss $\mathcal{H}$ on different PDMS samples vs. the Si mold roughness on which the PDMS samples were cast, measured using (a) AFM and (b) Nanoindentation apparatus. The different curves correspond to different maximum indentation depths ($|h_{\min}|$). For each $|h_{\min}|$, the $\mathcal{H}$ for a sample is the average of the data taken over five different locations separated by at least $200\mu m$. The error bars for $\mathcal{H}$ are the standard deviation of the data taken over the five locations. The error bars in (b) are not clearly visible as there are quite small ($\sim 10^{-2}\,\mathrm{pJ}$). The loading rate $\dot{d}$ for both (a) and (b) was $1000\,\mathrm{nm}\cdot\mathrm{s}^{-1}$. The insets in (a) show the qualitative nature of the contact region hypothesized in this work, in the small, and large roughness limits.

Figure 3. caption

(a) P-h curves predicted by a smooth-surface contact model [10] (dashed curve) and by the small roughness contact model studied in this paper (thick solid curve). Both curves are parameterized by the radius of the contact area. In an experiment in which h is prescribed, sudden changes in the contact area occur at the tip of every fold, such as from d to e. As a result, an experiment will measure only parts of its envelope (thin solid curve). (b) When the roughness length scale (λ) is much smaller than the radius of the indenter (R) the folds in the P-h curve are so close together that the envelope of the P-h curve can be described by Eqs. (1a) and (1b) (thick solid curve). (c)-(f) Contact shapes at different stages of loading/unloading marked in (a).

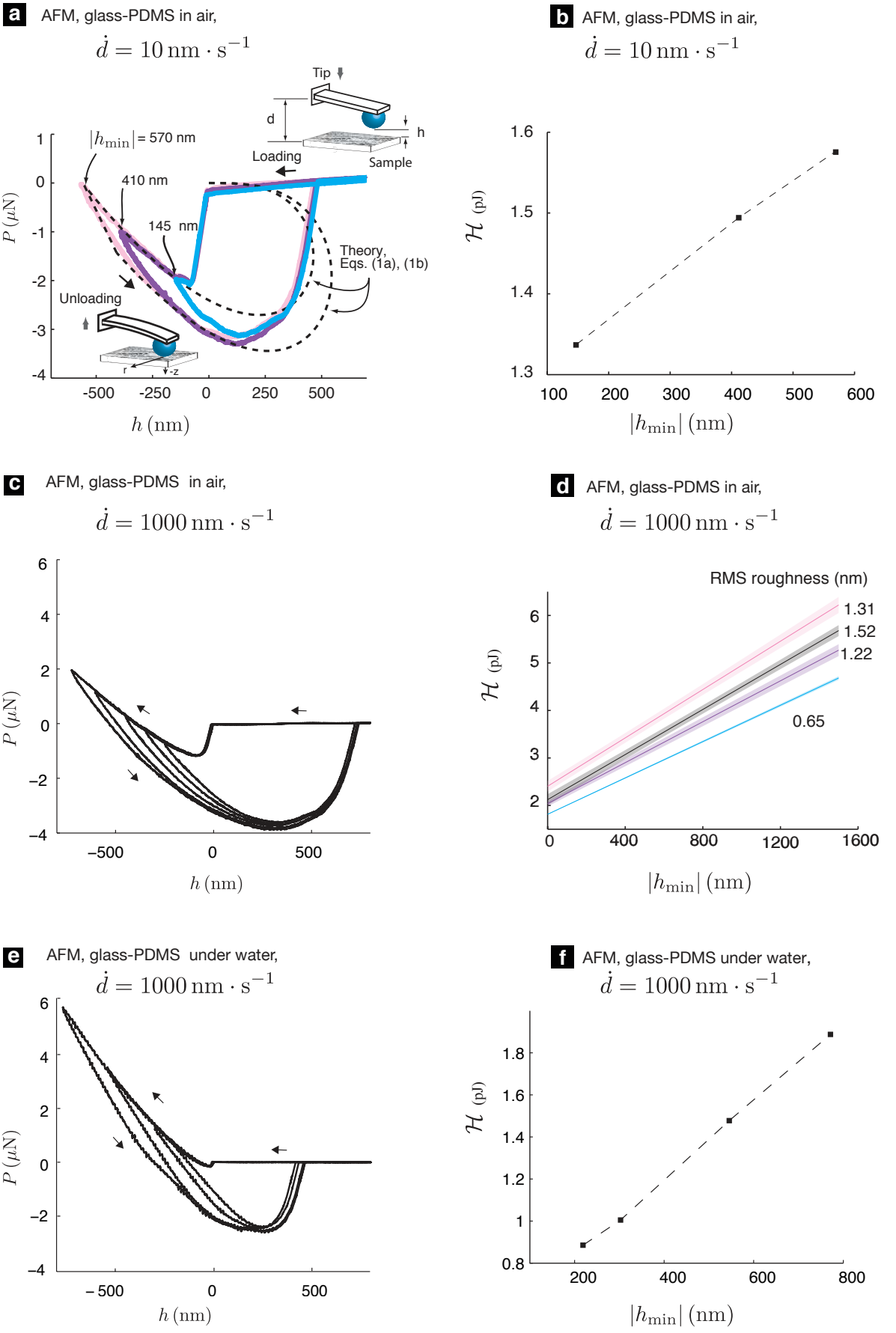
a
AFM, glass-PDMS in air,
$\dot{d} = 10\,\mathrm{nm}\cdot\mathrm{s}^{-1}$
Tip
d
h
Loading
Sample
$|h_{\min}| = 570$ nm
410 nm
145 nm
Theory,
Eqs. (1a), (1b)
Unloading
r
-z
$P\,(\mu N)$
$h\,(\mathrm{nm})$
b
AFM, glass-PDMS in air,
$\dot{d} = 10\,\mathrm{nm}\cdot\mathrm{s}^{-1}$
$\mathcal{H}$ (pJ)
$|h_{\min}|\,(\mathrm{nm})$
c
AFM, glass-PDMS in air,
$\dot{d} = 1000\,\mathrm{nm}\cdot\mathrm{s}^{-1}$
$P\,(\mu N)$
$h\,(\mathrm{nm})$
d
AFM, glass-PDMS in air,
$\dot{d} = 1000\,\mathrm{nm}\cdot\mathrm{s}^{-1}$
RMS roughness (nm)
1.31
1.52
1.22
0.65
$\mathcal{H}$ (pJ)
$|h_{\min}|\,(\mathrm{nm})$
e
AFM, glass-PDMS under water,
$\dot{d} = 1000\,\mathrm{nm}\cdot\mathrm{s}^{-1}$
$P\,(\mu N)$
$h\,(\mathrm{nm})$
f
AFM, glass-PDMS under water,
$\dot{d} = 1000\,\mathrm{nm}\cdot\mathrm{s}^{-1}$
$\mathcal{H}$ (pJ)
$|h_{\min}|\,(\mathrm{nm})$

Figure 1

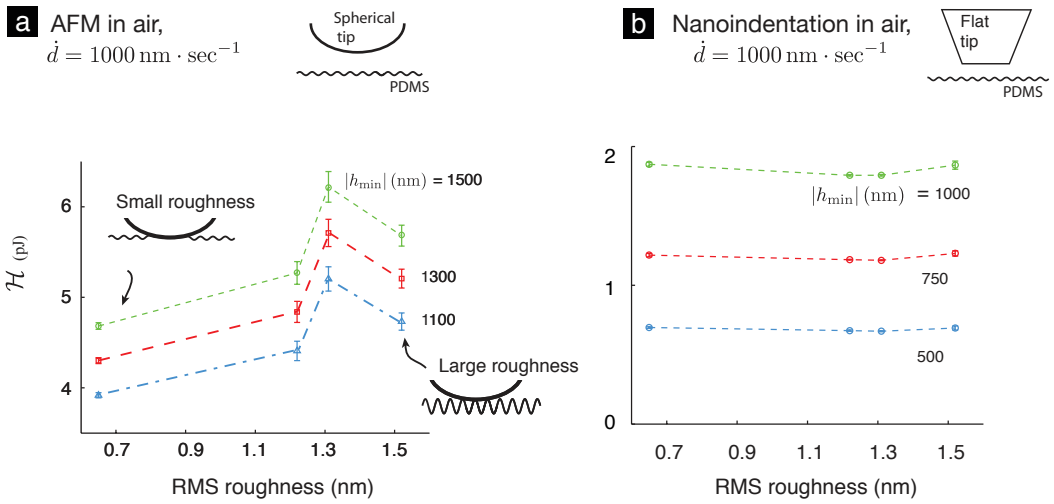
a
AFM in air,
$\dot{d} = 1000\,\mathrm{nm}\cdot\mathrm{sec}^{-1}$
Spherical tip
PDMS
b
Nanoindentation in air,
$\dot{d} = 1000\,\mathrm{nm}\cdot\mathrm{sec}^{-1}$
Flat tip
PDMS
Small roughness
Large roughness
$|h_{\min}|\,(\mathrm{nm})$ = 1500
1300
1100
$\mathcal{H}$ (pl)
RMS roughness (nm)
$|h_{\min}|\,(\mathrm{nm})$ = 1000
750
500
RMS roughness (nm)

Figure 2

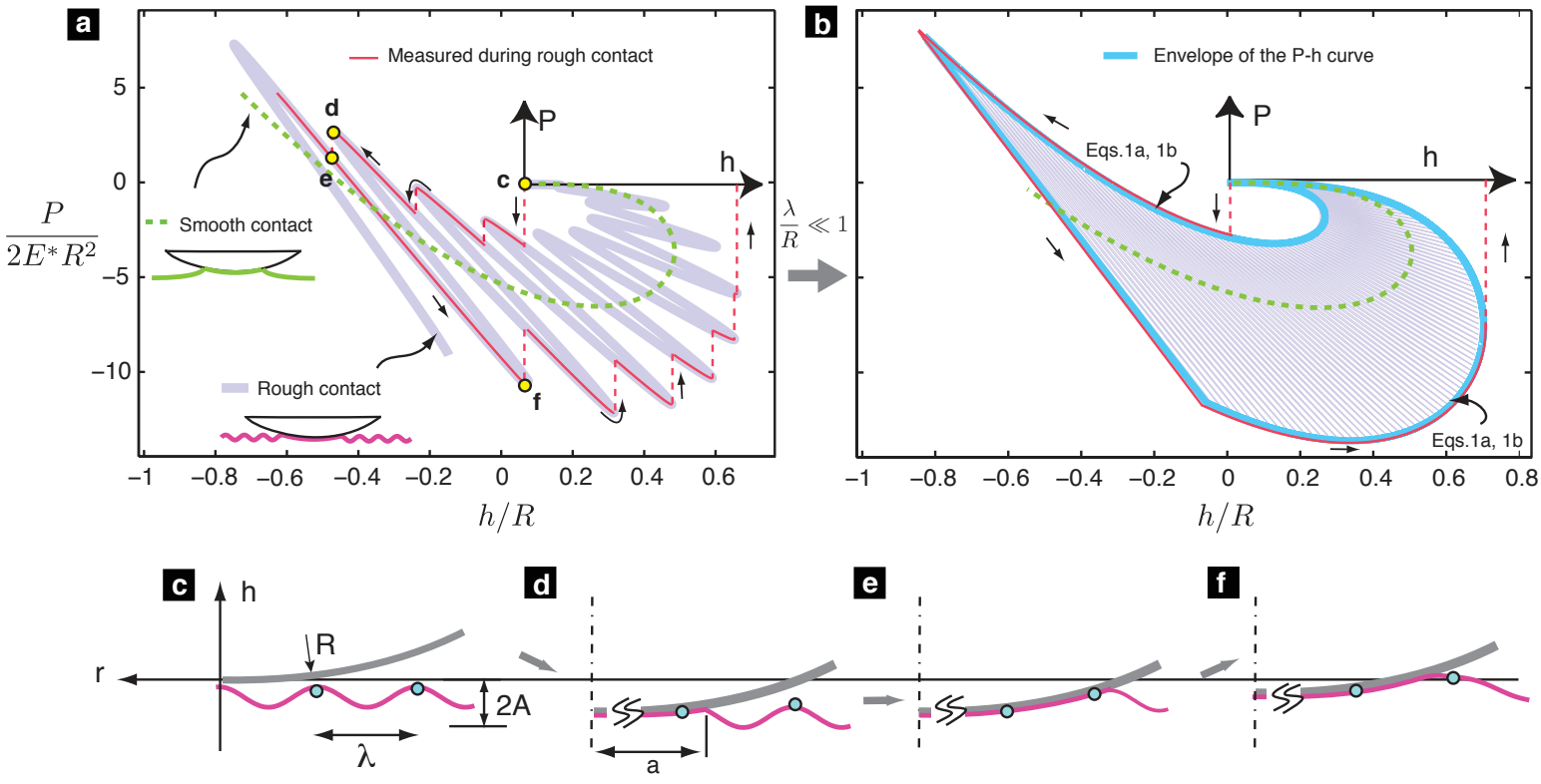
a
b
Measured during rough contact
Envelope of the P-h curve
Smooth contact
Rough contact
Eqs.1a, 1b
Eqs.1a, 1b
P
h
d
e
c
f
$\frac{P}{2E^*R^2}$
h/R
$\frac{\lambda}{R} \ll 1$
c
d
e
f
h
R
r
2A
λ
a

Figure 3